Light cone tensor network and time evolution

Miguel Frías-Pérez[1,2,*] and Mari Carmen Bañuls[1,2]
[1]*Max-Planck-Institut für Quantenoptik, Hans-Kopfermann-Strasse 1, D-85748 Garching, Germany*
[2]*Munich Center for Quantum Science and Technology (MCQST), Schellingstrasse 4, D-80799 München, Germany*

(Received 2 February 2022; accepted 26 July 2022; published 12 September 2022)

The transverse folding algorithm [M. C. Bañuls *et al.*, Phys. Rev. Lett. **102**, 240603 (2009)] is a tensor network method to compute time-dependent local observables in out-of-equilibrium quantum spin chains that can overcome the limitations of matrix product states when entanglement grows slower in the time than in the space direction. We present a contraction strategy that makes use of the exact light cone structure of the tensor network representing the observables. The strategy can be combined with the hybrid truncation proposed for global quenches by Hastings and Mahajan Phys. Rev. A **91**, 032306 (2015), which significantly improves the efficiency of the method. We demonstrate the performance of this *transverse light cone contraction* also for transport coefficients, and discuss how it can be extended to other dynamical quantities.

DOI: 10.1103/PhysRevB.106.115117

I. INTRODUCTION

In the last decade, tensor networks (TNs) [1–3] have gained a prominent role among numerical methods for quantum many-body systems. Simulating the dynamics of out-of-equilibrium systems remains nevertheless one of the most challenging open problems for these (and other) techniques.

In one-dimensional systems, the limitations of TN methods for dynamics are well understood: In global quenches the entanglement may grow fast [4–6], and the true state can escape the descriptive power of the TN ansatz. This so-called entanglement barrier limits the applicability of the matrix product state (MPS) [7–10] description, and makes it difficult to predict the asymptotic long-time behavior, even when local observables in this limit are expected to be well described by a thermodynamic ensemble, itself well approximated by a matrix product operator (MPO) [11–16]. A number of methods have been suggested to try to overcome this issue and extract information about the long-time behavior of local properties [17–27]. While there is no universal solution, understanding the entanglement structures in the evolution TN can be crucial to identify the most adequate one for practical computations.

In particular, the transverse folding strategy [18,28,29] avoids the explicit representation of the evolved state as a MPS and instead focuses on contracting a TN that represents exactly (up to Trotter errors) the time-dependent observables. Instead of the standard evolution in time direction, the folding algorithm contracts the TN along space. In some scenarios, this allows local observables to be computed to longer times than other approaches [30], and it is an exact strategy for certain models [31]. Recently, there has been a rekindled interest in this approach, triggered by the interpretation of the network in terms of an influence functional [32–34].

In local lattice models, the velocity of propagation of information is upper bounded [35–37] and the exact TN for observables has a light cone structure. While there have been proposals that exploit this fact to reduce the cost of the numerical simulation of the evolved state with TN [38–43], and with quantum simulation [44], until now, the potential of combining it with the transverse strategy has not been explored.

Here, we propose a strategy to exploit this property, a *transverse light cone contraction* (TLCC) of the TN. As in the original transverse folding, the TLCC does not directly suffer from the entanglement growth in the state, and will be more efficient than standard algorithms when entanglement in the time direction grows slower than in the spatial one. But the TLCC improves the efficiency with respect to the transverse folding in all cases, by reducing the computational effort to that of approximating the minimal network describing the time-dependent observables in a Trotterized evolution. We demonstrate explicitly its performance for global quenches and different-time thermal correlators at infinite temperature, and investigate how the strategy can make use of the (more efficient) physical light cone determined by the Lieb-Robinson velocity [36]. We discuss possible extensions to other interesting quantities.

II. LIGHT CONE TENSOR NETWORK FOR GLOBAL QUENCHES

The one-dimensional global quench is a natural test bench for time-evolution TN algorithms. At time $t = 0$ the system is prepared in a state that can be written as a MPS (e.g., a product state), and then it is allowed to evolve under a fixed Hamiltonian. For simplicity, we restrict the discussion

*miguel.frias@mpq.mpg.de

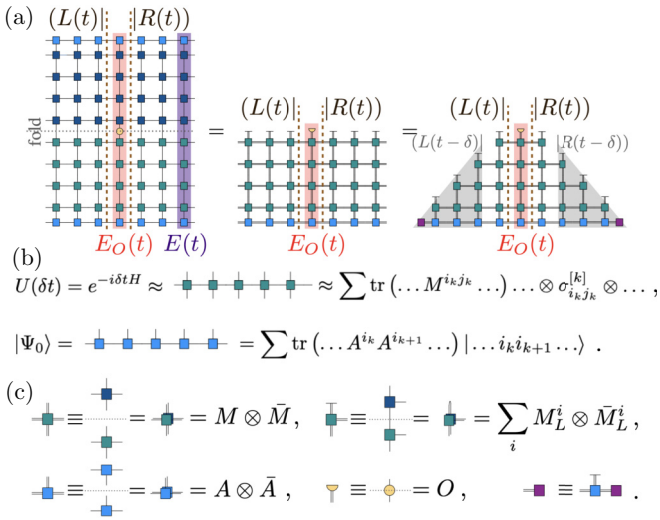

FIG. 1. (a), (b) Schematic construction of the minimal TN for the expectation value of a local operator O after a global quench in a translationally invariant setting. At time $t = M\delta$ the expectation value $\langle\Psi(t)|O|\Psi(t)\rangle$ corresponds to a two-dimensional TN. After folding, the exact light cone is obtained after removing the mutually canceling gates. (c) Graphical notation for folded TN diagrams throughout the paper.

to a nearest-neighbor model, and a translationally invariant case, but the construction generalizes straightforwardly to any model with local (finite-range) interactions and some non-translationally invariant scenarios.

The transverse folding proposal of Ref. [18] starts from a two-dimensional TN whose contraction represents some time-dependent observable, such as a local expectation value. This TN can be constructed from a Suzuki-Trotter approximation of the evolution operator, where the evolution for a discrete step of time δ can be approximated as a matrix product operator (MPO) [11,12] with a small bond dimension, constructed from a product of two-body gates [13]. The TN for the observable at time $t = M\delta$ is obtained by applying M copies of this MPO with the initial state, which yields the evolved state, and contracting the operator of interest between this and its adjoint.

While standard TN algorithms such as time-evolving block decimation (TEBD) or time-evolved MPS (tMPS) [11,47–49] compute the observable by contracting the network in the time direction, the transverse folding strategy performs the contraction in the spatial direction, after folding the TN in half, such that tensors for the same site and time step in the ket and the bra are grouped together [see Fig. 1(a)]. After folding, the growth of entanglement in the time direction can be slower than in the spatial one, with the most dramatic difference observed for integrable systems [28,46], but occurring also in generic cases, such as the ones shown here. When this difference in growth is present, the transverse strategy allows reaching longer times than standard algorithms.

For a translationally invariant system in the thermodynamic limit, the transverse contraction reduces to an expectation value of the form $(L(t)|E_O(t)|R(t))$, where $(L(t)|$ and $|R(t))$ are the dominant left and right eigenvectors of the transfer operator $E(t) = \sum_i \bar{A(t)}^i \otimes A^i(t)$, and $E_O(t) = \sum_i \bar{A(t)}^i \otimes A^j(t)\langle i|O|j\rangle$ [10]. Here, $A^i(t)$ represents the *concatenated* [50] local tensor of the time-dependent state, itself a MPO. In the transverse folding strategy, the boundary vectors $(L(t)|$ and $|R(t))$ are approximated by MPS. This approximation can be found, for instance, via a power iteration or a Lanczos algorithm, using repeated MPO-MPS contractions.

Such strategies do not take into account that the TN has a light cone structure. Because the individual gates are local, outside the causal cone of the operator, each gate cancels with its adjoint. This ensures that each of the required boundary vectors (dominant eigenvectors of the transfer operator) corresponds precisely to the contraction of a triangular network as depicted in Fig. 1. We can approximate directly the contraction of such a triangle in the space direction by a MPS. This strategy, which we call *transverse light cone contraction* (TLCC), allows us to obtain $(L(t)|$ and $|R(t))$ in a fixed number of steps (proportional to M). Furthermore, once we have found the vectors for M time steps, we can directly obtain them for $M + 1$ by applying a single MPO (as illustrated in the figure), which increases the length by one, and approximating the result via a single truncation step. This step can be performed using standard MPS truncation algorithms, which reduce the bond dimension by minimizing a distance between the truncated vector and the original one. However, for this particular problem the *hybrid* truncation algorithm proposed in Ref. [29], which effectively *evolves* the bond of the boundary vector according to the real time dynamics, yields a much more efficient use of the available bond dimension (see also insets of Fig. 2).

The TLCC strategy results in a more efficient algorithm than the originally proposed folding, which required iterative MPO-MPS contractions until convergence of the dominant eigenvectors, run independently for each different time step (in particular, for the cases analyzed in this work, we find the power iteration required several tens of MPO-MPS contractions per time step). Notice, nevertheless, that if the bond dimension used is large enough, both the original folding algorithm and the TLCC should result in the same boundary vector. What ultimately determines the applicability of transverse strategies is thus the amount of *entanglement* present in the transverse network.

To probe the performance of the method, we consider a quantum Ising chain, initialized in a product state $|X+\rangle = \lim_{N\to\infty}[(|0\rangle + |1\rangle)/\sqrt{2}]^{\otimes N}$. We then apply the Hamiltonian,

$$H_{\mathrm{I}} = \sum_i \left(J\sigma_i^z\sigma_{i+1}^z + g\sigma_i^x + h\sigma_i^z\right), \tag{1}$$

and compute local expectation values after time evolution. In all the following we fix $J = 1$, and a Trotter step $\delta = 0.1$, and vary the parameters of the model to study integrable ($g = \{0.5,\ 1\}, h = 0$) and nonintegrable ($g = -1.05, h = 0.5$) regimes. Figure 2 shows the results and demonstrates that the TLCC can efficiently simulate the integrable quenches. In the nonintegrable regime, the required bond dimension grows much faster with time, but the method is still advantageous as compared to standard evolution, much more so when the truncation is performed as in Ref. [29] [see the right inset of Fig. 2(c)].

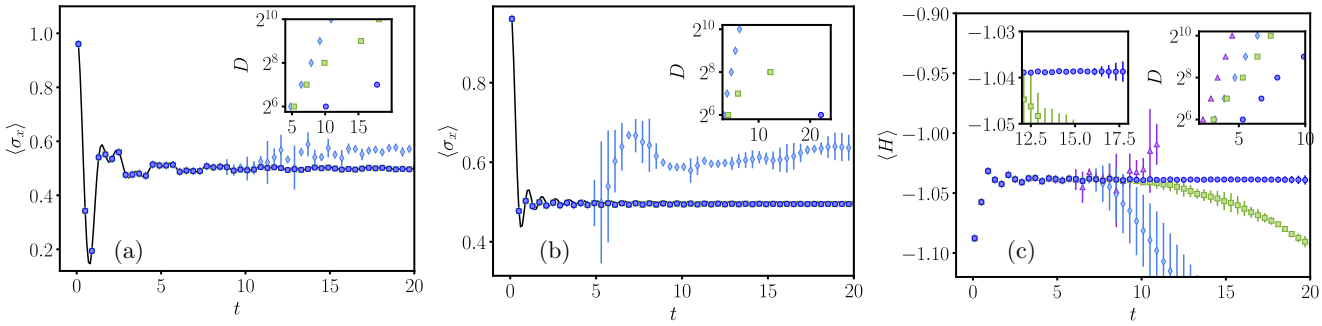

FIG. 2. Evolution after a global quench from the initial state $|X+\rangle$, for the integrable [(a) $g = 0.5$, (b) $g = 1$] and nonintegrable [(c) $g = -1.05$, $h = 0.5$] Ising model. The main plots show (a), (b) the transverse magnetization $\langle\sigma_x(t)\rangle$ and (c) the energy density, computed with different algorithms using respectively the bond dimension (a), (b) $D = 128$ and (c) 512. Error bars represent the difference with respect to the results obtained with $D' = D/2$. The TLCC contraction has been obtained both with the standard MPS truncation (green squares) and the hybrid truncation of Ref. [29] (dark blue circles). For comparison, we also show the results of standard infinite time-evolving block decimation (iTEBD) (blue diamonds) and Heisenberg picture density matrix renormalization group (DMRG) (purple triangles). The Heisenberg picture results are only shown in (c), since, in the integrable case, the operator in (a), (b) can be exactly written as an MPO with constant bond dimension at all times [17]. For the integrable case (a), (b) we show also the analytic result (black line). The insets show the scaling of the bond dimension required to keep constant precision in each algorithm [45]. In the integrable case, this is compatible (at the later times) with a polynomial increase $D \sim t^\alpha$, consistent with observations in Refs. [28,46]. In the nonintegrable case, the increase is compatible with an exponential growth for both truncation methods, but using the hybrid truncation exhibits a slower rate than standard ones, such that longer times can be reached with the same bond dimension. The left inset in (c) shows a zoom of the main plot to better appreciate the differences.

III. LIGHT CONE TENSOR NETWORK FOR TRANSPORT COEFFICIENTS

The same idea can be adapted to the computation of other dynamical quantities. It is the case of thermal correlators, of the form $C_{1,2}(t,\ell,\beta) = \mathrm{tr}[\rho_\beta O_2^{[\ell]}(t) O_1^{[0]}(0)]$, where $\rho_\beta = e^{-\beta H}/Z$ is the thermal equilibrium state at inverse temperature β, $Z = \mathrm{tr}(e^{-\beta H})$ is the partition function, $O_k^{[\ell]}(t)$ is a (local) operator acting on site ℓ at time t, and $O_k(t) = U(t)^\dagger O_k U(t)$ is the time-evolved operator in the Heisenberg picture. Since $[\rho_\beta, H] = 0$, the thermal state is invariant under the evolution, and using $\rho_\beta \propto \rho_{\beta/2}\rho_{\beta/2}^\dagger$ we can write (up to normalization) $C_{1,2}(t,\ell,\beta) \propto \mathrm{tr}[U(t)^\dagger \rho_{\beta/2}^\dagger O_2^{[\ell]} U(t) O_1^{[0]} \rho_{\beta/2}]$. Using a MPO approximation to $\rho_{\beta/2}$ (obtained with standard TN methods [11,12,51,52]), and the Trotterized real time evolution as in the previous section, this quantity can be expressed as a two-dimensional folded TN, which can be contracted in the temporal [53–55] or spatial (transverse) [28] direction.

Due to the invariance of the thermal state, each local observable generates also a light cone structure that can be exploited in the TLCC approach. Now the cancellation of gates outside the causal cone of the operators occurs both at the upper and the lower parts of the network [see Fig. 3(a)], and the minimal TN has a rectangular form, resembling a pillow, a structure which was used in Ref. [56] to evaluate correlators in random quantum circuits. The TLCC strategy again requires contracting a triangular TN corresponding to the lateral corners of the figure to obtain boundary vectors $(L_\beta(t)|$ and $|R_\beta(t))$ [57]. If both operators act on the same site ($\ell = 0$), the time-dependent correlators can be expressed as a contraction $(L_\beta(t)|T_{\beta,O_1,O_2}(t)|R_\beta(t))$, with a single MPO $T_{\beta,O_1,O_2}(t)$ constructed from concatenating the local tensors for the unitaries, the operators, and the states [see Fig. 3(a)]. For correlators at nonzero distance ℓ the minimal TN becomes elongated [Fig. 3(a), lower diagrams]. To approximate its contraction, the boundary vectors $(L_\beta(t)|$ and $|R_\beta(t))$ for a certain time t are first grown to incorporate, respectively, O_1 at the bottom of the TN, and O_2 at the top. These extended vectors contain the evolution steps up to time $t + 2\delta$, and can be contracted together to obtain the correlators at $\ell = 1$ for times $t + 3\delta$ and $t + 4\delta$. The vectors can be then evolved again, following the TN structure, which does not increase their length, but allows access to correlators at any later time $t + (2 + k)\delta$ and distances $\ell = k, k + 1$. Applying this systematically we can obtain all nonvanishing correlators. This generalizes trivially to operators on more than one site, or with MPO structure.

Here, we illustrate the simplest case, infinite temperature, where $\rho_{\beta=0} \propto \mathbb{1}$ and the contour of the TN becomes uncorrelated. We consider the energy density operator

$$O_E^{[i]} := J\sigma_i^z\sigma_{i+1}^z + \frac{g}{2}\left(\sigma_i^x + \sigma_{i+1}^x\right) + \frac{h}{2}\left(\sigma_i^z + \sigma_{i+1}^z\right), \qquad (2)$$

which can be written as a MPO of range 2. Figure 3(b) shows our results for the correlators $C_{EE}(t,\ell,\beta = 0)$ as a function of time for several distances in the nonintegrable ($g = -1.05$, $h = 0.5$, main plot) and integrable ($g = 0.5$, $h = 0$, inset) cases [45].

Especially interesting is the possibility of *ab initio* calculations of transport properties [58] in nonintegrable models. In particular, diffusion constants can be related to the spatial spreading in time of autocorrelations of a density [22,59,60]. Normalizing the correlators as $\tilde{C}_{EE}(0,\ell) := C_{EE}(t,\ell)/\sum_\ell C_{EE}(0,\ell)$, a diffusion constant $\mathcal{D}(t)$ may be

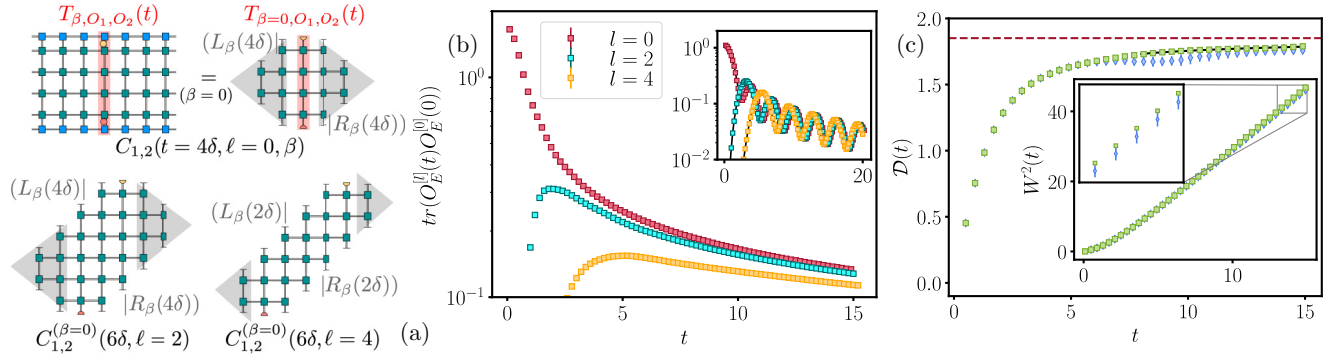

FIG. 3. (a) Schematic construction of the minimal TN for two-point correlators at infinite temperature for different times and distances [45]. (b) Energy autocorrelations $C_{EE}(t, \ell, \beta = 0)$ obtained from the TLCC method at several distances as a function of time in the integrable ($g = 0.5$, inset) and nonintegrable ($g = -1.05$, $h = 0.5$, main plot) Ising chain at $\beta = 0$. The error bars (smaller than the size of the marker) show the difference between results with two different bond dimensions (D, D') [for the inset (200, 100), for the main plot (500, 200)]. In the inset, the black curves represent the results coming from the analytical solution of the model. (c) Spatial variance 3 of the normalized autocorrelations (3) (inset) and corresponding diffusion constant (main plot) in the nonintegrable case obtained from the TLCC (green squares) and TEBD (blue diamonds) with $D = 1024$, with error bars showing the difference with respect to $D' = 512$. The solid black line in the main plot shows a fit of the form $\mathcal{D}_E \exp(b/t)$, which predicts the asymptotic value $\mathcal{D}_E \approx 1.9$ (red dotted line).

obtained from their spatial variance [59],

$$W^2(t) := \sum_{\ell} \tilde{C}_{EE}(t, \ell)\ell^2 - \left(\sum_{\ell} \tilde{C}_{EE}(t, \ell)\ell\right)^2, \qquad (3)$$

as $\frac{\partial W^2}{\partial t} = 2\mathcal{D}(t)$. Figure 3(c) shows the (linearly growing) variance $W^2(t)$ (main plot), and the corresponding diffusion constant (inset) obtained from the correlators for the nonintegrable case. The diffusion constant is well fitted by a function $\mathcal{D}(t) = \mathcal{D}_E \exp(b/t)$, compatible with saturation to a constant $\mathcal{D}_E \approx 1.9$ in the asymptotic regime [61]. While TEBD (blue diamonds) produces close values for the same quantities, the error is appreciable in the diffusion constant already at short times.

IV. THE PHYSICAL LIGHT CONE

In general, we expect that the physical light cone is much narrower than the trivial one from the Trotterization, used in the previous sections. We could thus approximate the TN by a light cone one in which the slope corresponds to the maximal physical velocity v_{LR}. This can be achieved by implementing a more efficient TLCC growing iteration, in which $n_{\mathrm{T}} = 1/(v_{\mathrm{LR}}\delta)$ time steps are applied at once every time a space site is contracted [Fig. 4(a)]. Notice that this light cone is not exact, but has (exponential) corrections. Thus it is convenient to consider the light cone for a subsystem of size L_{eff} that includes the support of the operator [62].

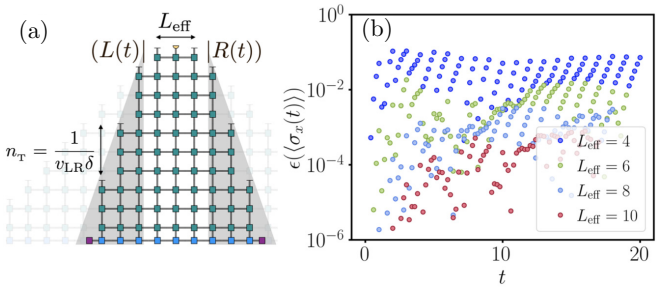

FIG. 4. (a) The physical velocity defines a much narrower light cone than the Trotterization (background). (b) Relative difference between $\langle\sigma_x\rangle$ computed with the LR and Trotter light cones for the integrable global quench of Fig. 2(a), for which $n_{\mathrm{T}} = 10$ and different sizes of the subsystem L_{eff}, with $D = 200$ in all cases.

To probe this reduced light cone we choose an integrable instance ($g = 0.5$, $h = 0$) for which the Lieb-Robinson (LR) velocity is known ($v_{\mathrm{LR}} = 1$, corresponding to $n_{\mathrm{T}} = 10$ with our Trotter step), and simulate the global quench of Fig. 2(a). Compared to TLCC for the full light cone with the same bond dimension, we observe (Fig. 4) that the physical one, determined by v_{LR}, captures indeed the correct evolution: While the narrower light cone deviates from full results, the errors are reduced exponentially (until the level of original truncation error) by considering a small window L_{eff}.

V. DISCUSSION

We have presented a strategy that builds on the transverse folding [18] to approximate time-dependent observables in a one-dimensional quantum system. Noticing the exact light cone structure of the TN and implementing its transverse contraction, it is possible to compute long-time properties in a more efficient manner. Combined with the hybrid truncation [29], this allows us to reach longer times with a smaller bond dimension whenever the temporal entanglement grows slower than the physical one, which, as we have seen, happens not only for integrable systems. It is possible to use the physical upper bound of the Lieb-Robinson velocity to further restrict the width of the relevant TN and define a more efficient iteration.

We have evaluated the performance of the TLCC strategy for integrable and nonintegrable global quenches, and for transport properties at infinite temperature. With minimal changes, the method extends to other scenarios, such as finite temperature or nontranslationally invariant setups including

impurities or a contact between two chains. It is furthermore possible to adapt the strategy to other more complex dynamical quantities.

The basic TLCC does not require an additional hypothesis to truncate observables or states. Its convergence can be systematically explored as the bond dimension is increased. What ultimately limits the validity of the strategy is the entanglement in the time direction, which strongly depends on the setup and the model [28,46,63]. The behavior of the TLCC can thus provide useful information to determine optimal strategies for different problems. Another parameter in the approximation is the Trotter step, which is known to affect the entanglement growth in standard algorithms [49]. Since simulations with different δ may be necessary to extrapolate the exact results, it is also interesting to study how varying δ affects our observations. Further interesting avenues for future investigation are exploring the TN cut according to different velocities, to explore the propagation of correlations in the TN, and effectively measure v_{LR}.

Recently, we became aware of an equivalent strategy for global quenches, which was independently suggested in Ref. [64].

ACKNOWLEDGMENTS

We are thankful to J. I. Cirac, M. Hastings, and L. Tagliacozzo for insightful discussions at different stages of this project. This work was partly supported by the Deutsche Forschungsgemeinschaft (DFG, German Research Foundation) under Germany's Excellence Strategy – EXC-2111 – 390814868. M.C.B. acknowledges the hospitality of KITP, where earlier versions of the work were developed, with support from the National Science Foundation under Grant No. NSF PHY-1748958.

[1] F. Verstraete, V. Murg, and J. Cirac, Adv. Phys. **57**, 143 (2008).
[2] U. Schollwöck, Ann. Phys. **326**, 96 (2011).
[3] R. Orús, Ann. Phys. **349**, 117 (2014).
[4] P. Calabrese and J. Cardy, J. Stat. Mech.: Theory Exp. (2005), P04010.
[5] T. J. Osborne, Phys. Rev. Lett. **97**, 157202 (2006).
[6] N. Schuch, M. M. Wolf, F. Verstraete, and J. I. Cirac, Phys. Rev. Lett. **100**, 030504 (2008).
[7] M. Fannes, B. Nachtergaele, and R. F. Werner, Commun. Math. Phys. **144**, 443 (1992).
[8] G. Vidal, Phys. Rev. Lett. **91**, 147902 (2003).
[9] F. Verstraete, D. Porras, and J. I. Cirac, Phys. Rev. Lett. **93**, 227205 (2004).
[10] D. Pérez-García, F. Verstraete, M. M. Wolf, and J. I. Cirac, Quantum Inf. Comput. **7**, 401 (2007).
[11] F. Verstraete, J. J. García-Ripoll, and J. I. Cirac, Phys. Rev. Lett. **93**, 207204 (2004).
[12] M. Zwolak and G. Vidal, Phys. Rev. Lett. **93**, 207205 (2004).
[13] B. Pirvu, V. Murg, J. I. Cirac, and F. Verstraete, New J. Phys. **12**, 025012 (2010).
[14] M. B. Hastings, Phys. Rev. B **73**, 085115 (2006).
[15] A. Molnar, N. Schuch, F. Verstraete, and J. I. Cirac, Phys. Rev. B **91**, 045138 (2015).
[16] T. Kuwahara, A. M. Alhambra, and A. Anshu, Phys. Rev. X **11**, 011047 (2021).
[17] M. J. Hartmann, J. Prior, S. R. Clark, and M. B. Plenio, Phys. Rev. Lett. **102**, 057202 (2009).
[18] M. C. Bañuls, M. B. Hastings, F. Verstraete, and J. I. Cirac, Phys. Rev. Lett. **102**, 240603 (2009).
[19] T. Prosen and M. Žnidarič, Phys. Rev. E **75**, 015202(R) (2007).
[20] D. Muth, R. G. Unanyan, and M. Fleischhauer, Phys. Rev. Lett. **106**, 077202 (2011).
[21] C. D. White, M. Zaletel, R. S. K. Mong, and G. Refael, Phys. Rev. B **97**, 035127 (2018).
[22] T. Rakovszky, C. W. von Keyserlingk, and F. Pollmann, Phys. Rev. B **105**, 075131 (2022).
[23] C. Krumnow, J. Eisert, and Ö. Legeza, arXiv:1904.11999.
[24] J. Surace, M. Piani, and L. Tagliacozzo, Phys. Rev. B **99**, 235115 (2019).
[25] M. M. Rams and M. Zwolak, Phys. Rev. Lett. **124**, 137701 (2020).
[26] J. Lopez-Piqueres, B. Ware, S. Gopalakrishnan, and R. Vasseur, Phys. Rev. B **104**, 104307 (2021).
[27] T. K. Kvorning, L. Herviou, and J. H. Bardarson, arXiv:2105.11206.
[28] A. Müller-Hermes, J. I. Cirac, and M. C. Bañuls, New J. Phys. **14**, 075003 (2012).
[29] M. B. Hastings and R. Mahajan, Phys. Rev. A **91**, 032306 (2015).
[30] M. C. Bañuls, J. I. Cirac, and M. B. Hastings, Phys. Rev. Lett. **106**, 050405 (2011).
[31] L. Piroli, B. Bertini, J. I. Cirac, and T. Prosen, Phys. Rev. B **101**, 094304 (2020).
[32] M. Sonner, A. Lerose, and D. A. Abanin, Ann. Phys. **435**, 168677 (2021).
[33] A. Lerose, M. Sonner, and D. A. Abanin, Phys. Rev. X **11**, 021040 (2021).
[34] E. Ye and G. K.-L. Chan, J. Chem. Phys. **155**, 044104 (2021).
[35] E. H. Lieb and D. W. Robinson, Commun. Math. Phys. **28**, 251 (1972).
[36] M. B. Hastings and T. Koma, Commun. Math. Phys. **265**, 781 (2006).
[37] B. Nachtergaele and R. Sims, Commun. Math. Phys. **265**, 119 (2006).
[38] M. B. Hastings, J. Math. Phys. **50**, 095207 (2009).
[39] T. Enss and J. Sirker, New J. Phys. **14**, 023008 (2012).
[40] E. Gillman, F. Carollo, and I. Lesanovsky, Phys. Rev. A **103**, L040201 (2021).
[41] V. Zauner, M. Ganahl, H. G. Evertz, and T. Nishino, J. Phys.: Condens. Matter **27**, 425602 (2015).
[42] H. N. Phien, G. Vidal, and I. P. McCulloch, Phys. Rev. B **88**, 035103 (2013).
[43] A. Milsted, J. Haegeman, T. J. Osborne, and F. Verstraete, Phys. Rev. B **88**, 155116 (2013).
[44] J. Haah, M. B. Hastings, R. Kothari, and G. H. Low, SIAM J. Comput., (2018).
[45] See Supplemental Material at http://link.aps.org/supplemental/10.1103/PhysRevB.106.115117 for a more detailed

explanation on how to construct the TN for the thermal response functions, a detailed analysis of the errors in the different algorithms, and results for different values of the couplings.

[46] G. Giudice, G. Giudici, M. Sonner, J. Thoenniss, A. Lerose, D. A. Abanin, and L. Piroli, Phys. Rev. Lett. **128**, 220401 (2022).

[47] G. Vidal, Phys. Rev. Lett. **93**, 040502 (2004).

[48] G. Vidal, Phys. Rev. Lett. **98**, 070201 (2007).

[49] S. Paeckel, T. Köhler, A. Swoboda, S. R. Manmana, U. Schollwöck, and C. Hubig, Ann. Phys. **411**, 167998 (2019).

[50] R. Hübener, V. Nebendahl, and W. Dür, New J. Phys. **12**, 025004 (2010).

[51] A. E. Feiguin and S. R. White, Phys. Rev. B **72**, 220401(R) (2005).

[52] B.-B. Chen, L. Chen, Z. Chen, W. Li, and A. Weichselbaum, Phys. Rev. X **8**, 031082 (2018).

[53] T. Barthel, U. Schollwöck, and S. Sachdev, arXiv:1212.3570.

[54] C. Karrasch, J. H. Bardarson, and J. E. Moore, Phys. Rev. Lett. **108**, 227206 (2012).

[55] T. Barthel, New J. Phys. **15**, 073010 (2013).

[56] C. Sünderhauf, D. Pérez-García, D. A. Huse, N. Schuch, and J. I. Cirac, Phys. Rev. B **98**, 134204 (2018).

[57] Different from the global quench above, in this case each iteration of the algorithm grows the boundary vectors in two time steps.

[58] B. Bertini, F. Heidrich-Meisner, C. Karrasch, T. Prosen, R. Steinigeweg, and M. Žnidarič, Rev. Mod. Phys. **93**, 025003 (2021).

[59] R. Steinigeweg, H. Wichterich, and J. Gemmer, Europhys. Lett. **88**, 10004 (2009).

[60] H. Kim and D. A. Huse, Phys. Rev. Lett. **111**, 127205 (2013).

[61] The fit $D(t) = \mathcal{D}_E \exp(b/t)$ is a heuristic choice that describes our data well over a range of fitting windows and allows us to extrapolate to the limit of infinite time. We have also tried successfully fits with polynomials of $1/t$, and found compatible results.

[62] Equivalently, we can *insert* in the middle of the column, corresponding to an earlier time.

[63] A. Lerose, M. Sonner, and D. A. Abanin, Phys. Rev. B **104**, 035137 (2021).

[64] A. Lerose, M. Sonner, and D. A. Abanin, arXiv:2201.04150.